Photoacoustics 40 (2024) 100661

Contents lists available at ScienceDirect

Photoacoustics

journal homepage: www.elsevier.com/locate/pacs

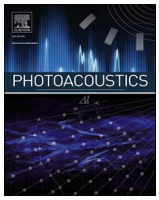

No document header

Quantitative evaluation of microenvironmental changes and efficacy of cupping therapy under different pressures based on photoacoustic imaging

Ping Zhang [a,b,1], Jing Lv [c,1], Cuihong Ge [a,b,1], Bo Yu [d], Yang Qiu [c], Aoji Qin [c], Zhu Ai [b], Zhehao Wu [a,b], Liming Nie [c,*], Zhiming Xiang [a,b,**]

[a] Postgraduate cultivation base of Guangzhou University of Chinese Medicine, Panyu Central Hospital, Guangzhou 510000, China
[b] Department of Radiology, The Affiliated Panyu Central Hospital of Guangzhou Medical University, Guangzhou 510000, China
[c] Medical Research Institute, Guangdong Provincial People's Hospital, Guangdong Academy of Medical Sciences, Southern Medical University, Guangzhou 510080, China
[d] Department of Ultrasound, The Second Affiliated Hospital of Harbin Medical University, Ultrasound Molecular Imaging Joint Laboratory of Heilongjiang Province, Harbin 150081, China

ARTICLE INFO

Keywords:
Cupping Therapy
Photoacoustic Imaging
Microenvironmental Changes
Lymphatic Drainage
Different negative pressures
Sepsis Outcomes

ABSTRACT

Cupping therapy, a traditional Chinese medicinal practice, has been subjected to scientific scrutiny to validate its effects on local tissue microenvironments. This study provides a quantitative assessment of cupping therapy at different negative pressures using photoacoustic imaging. Low-pressure cupping (-20 kPa) significantly improved local blood circulation, evidenced by increased hemoglobin oxygen saturation and vessel dilation that normalized within two hours. In contrast, high-pressure cupping (-30 kPa) led to capillary rupture, bleeding, and tissue edema, similar to the clinical presentation of cupping bruises. Additionally, our research unveiled that −20 kPa cupping expedited the clearance of indocyanine green dye, suggesting enhanced lymphatic drainage, which was further supported by fluorescence imaging. This indicates a potential mechanism for cupping's pain relief effects. Moreover, cupping showed promising results in improving sepsis outcomes in mice, potentially due to its anti-inflammatory properties. This study establishes a foundation for the objective evaluation of cupping therapy, demonstrating that low-pressure cupping is effective in promoting blood and lymphatic flow while minimizing tissue damage, thereby offering a safer therapeutic approach.

1. Introduction

Cupping therapy, a traditional Chinese medicine technique, has a history of thousands of years and is widely practiced in countries such as China, South Korea, Japan [1,2]. This therapy involves creating negative pressure by expelling air through combustion or suction from a cup placed on the skin, leading to local tissue congestion or mild subcutaneous congestion[1]. This process enhances the body's qi and blood circulation, promotes smooth meridians, alleviates pain, reduces swelling and nodules, dispels wind and cold, and clears heat and detoxifies [Standard Operating Procedures for acupuncture and moxibustion and Massage - Part 5: Cupping Therapy (GB/T 21709.5–2008)]. Due to its simplicity, effectiveness, low cost, and lack of adverse effects, cupping therapy has been widely used in the treatment of muscle pain[3,4], herpes zoster[5], cough or asthma, acne, common cold, urticaria, plate psoriasis and other diseases[6].

However, despite its popularity, the effectiveness of cupping therapy remains highly controversial in the modern medical evaluation system. Different practitioners apply varying pressures and durations, leading to widely varying therapeutic outcomes. Current assessments mainly rely on subjective feelings and verbal descriptions, such as pain scores[3]and visual analog scales[7], lacking rigorous evidence-based research, objective standards, and a systematic evaluation system. Moreover, the mechanism of action of cupping therapy still lacks a clear consensus. Modern research indicates that increased local blood flow might be a key therapeutic mechanism of cupping[8]. In recent years, some researchers have utilized parameters obtained through optical sensing tools to study the effects of cupping therapy. These studies have primarily focused on post-cupping skin discoloration[9], skin temperature[3,10],blood flow velocity [11], and local oxygen metabolism[12,13], and changes in

* Corresponding author.
** Corresponding author at: Postgraduate cultivation base of Guangzhou University of Chinese Medicine, Panyu Central Hospital, Guangzhou 510000, China.
E-mail addresses: nieliming@gdph.org.cn (L. Nie), xiangzhiming@pyhospital.com.cn (Z. Xiang).
[1] These authors contributed equally to this work.

https://doi.org/10.1016/j.pacs.2024.100661
Received 27 June 2024; Received in revised form 12 October 2024; Accepted 29 October 2024
Available online 30 October 2024

subcutaneous vascular morphology[14]. These indicators not only help quantify the therapeutic effects to some extent but also provide insights into the mechanisms of action behind cupping therapy. However, these studies have only focused on one or two indicators and have not conducted more in-depth explorations into the pressure or duration of cupping. These studies could not form strong evidence to guide subsequent research into the pressure or duration on cupping.

Photoacoustic (PA) imaging offers higher spatial resolution, enabling the observation of cupping's effects on local microvessels at a microscopic scale[15,16]. It can concurrently obtain hemodynamic parameters of the corresponding areas, achieving integration of structural and functional imaging[17,18]. This study aims to fill this gap by using PA imaging to quantitatively assess microenvironmental changes under different pressures during cupping therapy. In this experiment, we employed an experimental design to accurately quantify cupping pressure. Specifically, we will compare the effects of low-pressure (−20 kPa) and high-pressure (−30 kPa) cupping on blood circulation, hemoglobin oxygen saturation (Fig. 1). Additionally, with the help of the exogenous dye indocyanine green (ICG), we were able to uncover the effects of cupping on the lymphatic system from both microscopic and macroscopic perspectives for the first time. We hypothesize that high-pressure (−30 kPa) cupping offers better therapeutic effects than low-pressure (−20 kPa) cupping. By carefully selecting appropriate disease model, this study provides the first comprehensive evaluation of the therapeutic effects of cupping at different pressures. By providing objective and quantifiable data, this study seeks to establish a more systematic and evidence-based understanding of cupping therapy, potentially guiding its clinical application and optimization.

2. Material and methods

2.1. Preparation of animals

Rabbits were obtained from the Guangzhou Karot Biotechnology Corporation, and mice were purchased from Zhuhai BesTest Bio-Tech Co,.Ltd. The animals were housed at ambient temperature (22–26 °C) and relative humidity (40–70 %) under 12 h light/dark cycles with free access to food (standard mouse chow) and water. All animal received humane care in compliance with institutional and national guidelines. All the experimental procedures involving mice and rabbits were approved by the ethics committee of Guangdong provincial people's hospital, and complied with all relevant ethical regulations.

The New Zealand White male rabbits (4 weeks old) and ICR male mice (8 weeks old) underwent imaging preparations 24 hours in advance. The imaging area was shaved using a shaver and treated with depilatory cream for 30 seconds to remove surface hair. Before imaging, the animals were anesthetized with 2 % isoflurane, secured on the platform with tape, the imaging site was raised using a transparent acrylic step, flattened as much as possible, and ultrasound gel was applied on the surface. A heating pad was placed underneath the animals to maintain their body temperature close to 37 °C during imaging.

For the construction of the sepsis model, 8-week-old C57BL/6 male mice were used. According to the experimental requirements, the mice were randomly divided into four groups: the sham surgery group (Sham), the cecal ligation and puncture group (CLP), the −20 kPa pretreatment group (-20 kPa+ CLP), and the −30 kPa pretreatment group (-30 kPa+ CLP). These mice were adaptively fed for one week before the experiment. On the 8th day, the back hair of the mice was removed using

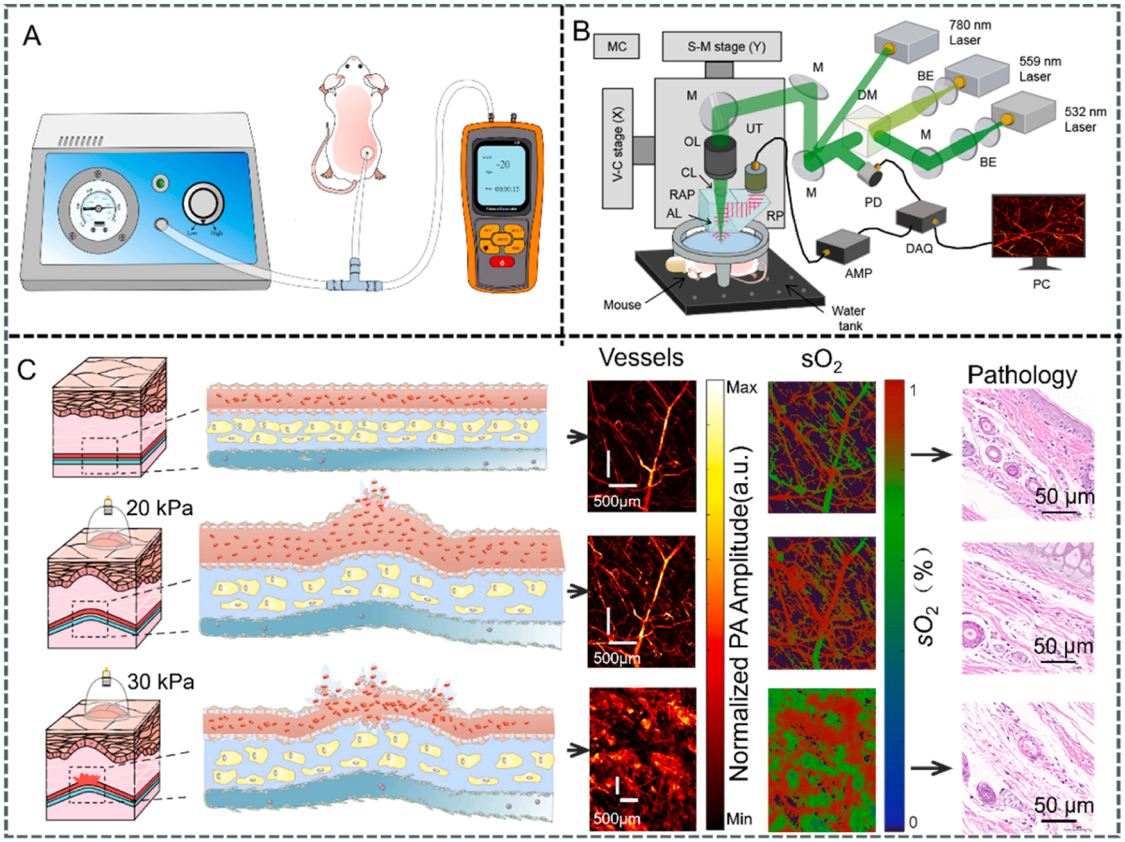

Fig. 1. Cupping Promotes Blood Circulation and Lymphatic Circulation, Activating the Body's Immune System (A) Self-assemble a cupping device; (B) Custom-designed OR-PAM; MC, motion controller; V-C stage (X), Voice-coil stage (X); S-M stage (Y), Stepper motor stage (Y); OL, objective lens; UT, ultrasonic transducer; AL, acoustic lens; CL, correction lens; M, mirror; NC, nose cone; RAP, right-angle prism; RP, rhomboid prism; DM, dichroic mirror; PD, Photodiode; BE, beam expander; AMP, amplifier; DAQ, data acquisition card; PC, personal Computer. (C) Schematic of the photoacoustic-based post-cupping skin microenvironment monitoring system.

a shaver and depilatory cream. On the 9th day, based on the experimental needs, the mice were treated with −20 kPa or −30 kPa cupping therapy for 5 minutes on the dorsal skin , or left untreated. The treatment continued for 7 days. On the 16th day, all mice were anesthetized, and their abdomens were skinned, disinfected, and draped. An incision of about 1.5 cm was made in the lower abdomen along the abdominal midline. The cecum root was ligated with a 4–0 suture, and the cecum was punctured once with an 18 G needle to evacuate the content, and then the peritoneum and skin were sutured[19,20]. Subsequently, preheated saline (37°C, 1 mL) as injected subcutaneously into the back of the neck of the mice. The mice were rewarmed for an hour, and then returned to a cage with water and food. In the sham operation group, only one abdominal incision was made, but the cecum was not ligated or punctured.

2.2. Cupping therapy device

In our cupping therapy device setup, we selected a silicone cup with an outer diameter of 15 mm, inner diameter of 7 mm, and a cup length of 50 mm. This configuration results in a cupping area of approximately 38.47 mm^2. The device includes a T-shaped three-way connector, where the first port connects to a DGN-6 multifunctional negative pressure vacuum pump to apply the desired negative pressure. The second port is connected to the silicone cup, which is applied to the skin. The third port is linked to a digital pressure gauge (Smart Sensor GM510, China) for continuous monitoring and real-time adjustment of the pressure inside the cup, ensuring it remains at −20±1 kPa or −30±1 kPa as required (Fig. 1A). Different pressure levels were applied for cupping for a duration of 5 minutes, depending on the specific groups in the study.

2.3. Optical imaging system

Photoacoustic microscopy (PAM) was performed using a commercial tunable optical and acoustic resolution PAM system (G2, INNO LASER, China), equipped with multi-wavelength lasers operating at 532 nm, 559 nm, and 750–840 nm (Fig. 1B). The acoustic signals generated by laser irradiation of the tissue were received by a 50 MHz ultrasound transducer, providing an optical resolution of 5 μm and an acoustic resolution of 40 μm.

Fluorescence imaging is conducted using the IVIS Spectrum system (PerkinElmer, USA). Imaging utilized the ICG channel, with the excitation filter set to 745 nm and the emission filter set to 840 nm.

2.4. Experimental procedure

2.4.1. Imaging of the blood system with PAM at dual wavelengths (532 nm and 559 nm)

Baseline PA images were obtained from the flatter area of the rabbit ear before cupping. After scanning, cupping was performed on the ears of the rabbits in the cupping group. Post-cupping, the rabbits were placed back under the PA probe to observe changes, and the acquired data were used to reconstruct the images (Fig. 1C). Image processing was conducted using MATLAB 9.8 software (R2020a, MathWorks).

Laser pulses at two different wavelengths (532 nm and 559 nm) were used to image vascular structures and functions. The 532 nm wavelength corresponds to the equal absorption point of deoxygenated hemoglobin and oxyhemoglobin, making the PA signal amplitude at 532 nm reflective of total hemoglobin concentration[21]. The 559 nm wavelength provides high contrast to differentiate signals from oxygenated and deoxygenated hemoglobin[22]. Spectral unmixing of photoacoustic images at 532 nm and 559 nm was conducted to calculate sO_2, using the formula[23]:

$$sO_2 = HbO_2/(HbO_2 + HbR) \quad (1)$$

For quantitative analysis, the target blood vessel was manually selected. Vessel diameter (μm) was estimated by the full width at half maximum (FWHM) value of the blood vessel signal in each B-scan[24]. Vascular density (VD) was calculated by binarizing images based on MATLAB software, as previously reported[24]. Initially, the original MAP PA image was filtered and enhanced to achieve optimal contrast, removing false negative pixels. Vessel segmentation was performed through threshold processing, resulting in image binarization with a uniform threshold value of 0.3. *VD* reflected the quantity of vessel distribution in a specific area and was defined as:

VD = Number of pixels occupied by vessels / Total number of pixels in the observation area (2)

The average signal intensity from the bleeding region was extracted and set as the threshold. Areas with signal intensity greater than the threshold were identified as bleeding regions. The bleeding area ratio (*BAR*) was defined as:

BAR= Number of pixels occupied by bleeding / Total number of pixels in the observation area (3)

2.4.2. Microscopical imaging the lymphatic system with PAM at 780 nm

We selected the 780 nm wavelength due to its strong absorption peak for ICG to observe its clearance through the lymphatic system. Considering the imaging depth limitations, we opted for ICR mouse ears instead of rabbit ears, as the latter might be too thick for effective observation. Initially, we imaged the mouse ears at 532 nm to localize the vessels. We then used the 780 nm wavelength to collect baseline PA images. The 5 μL syringe (Hamilton) could be directly connected to the 33-gauge needle (Hamilton). Following this, 0.6 μL of ICG solution (100 μg/mL) was subcutaneously injected into the mouse ear[25]. After position calibration, we collected images at 15 minutes and 30 minutes post-injection, respectively.

At the 30-minute mark, mice in the cupping group were removed from the PAM, subjected to cupping at −20 kPa for 5 minutes, and then immediately repositioned under the PAM for imaging. We collected images 60 minutes post-ICG injection and subsequently every 15 minutes over a total observation period of 2 hours (Fig. 4D). To characterize ICG retention in the ear, we selected an area of interest and calculated the PA signal amplitude within it. The average signal amplitude in this region was defined as follows:

Average PA signal amplitude= The *sum of photoacoustic amplitude/* Total number of pixels in the observation area (4)

To quantify the clearance rate of ICG by the lymphatic system, we defined the PA signal amplitude of ICG at different time points as P_t. The clearance rate was calculated using the following formula:

$$Clearance\ Rate = (P_t - P_{t+15\ min}) / P_t \quad (5)$$

2.4.3. Macroscopic imaging of the lymphatic system with IVIS Spectrum system

The right hind limb of the mice was shaved 24 hours prior to the experiment. Following anesthesia, the mice were positioned on their left side to expose the right hind limb for imaging. A volume of 5 μLof 1CG solution (1 mg of ICG dissolved in 1 mL of Phosphate-Buffered Saline) was injected into the footpad of the right hind limb, and immediate fluorescence imaging was conducted within one minute. For the cupping group of mice, cupping therapy was performed near the right hind limb, applying −20 kPa pressure for 5 minutes, followed by immediate imaging. Subsequent imaging sessions occurred every 5 minutes, with continuous monitoring over a 4-hour period (as shown in Fig. 5 A).

Image post-processing was performed using Living Image 4.4 software. The lymph node area was delineated as the region of interest

(ROI), while an equally sized area of skin surrounding the lymph node was designated as the background signal. The signal-to-background ratio (SBR) was defined as:

SBR=Fluorescence intensity of ROI / Fluorescence intensity of the background signal (6)

The time when SBR $\geq$ 2 is first reached is defined as T_{in}, and the time when the maximum fluorescence intensity of the lymph node is reached is defined as T_{max}.

2.5. Statistical analysis

SPSS software (IBM version 26) was used for statistical analysis. The normality of the data distribution was assessed for each group. For comparisons between two groups, an independent samples T-test was used if the data followed a normal distribution. If the data did not follow a normal distribution, a non-parametric test (*Mann-Whitney U test*) was applied. For analyzing differences across multiple groups, a *one-way ANOVA* was used if the data were normally distributed or only slightly skewed. For data that did not conform to a normal distribution, the *Kruskal-Wallis H test* (a non-parametric method) was employed. Results are presented as mean ± standard deviation (SD) or mean ± standard error(SEM). A *P*-value of less than 0.05 was considered to indicate statistical significance.

3. Results

3.1. Cupping therapy with low-pressure (-20 kPa) can promote blood circulation

The average PA signal amplitude of the image 15 minutes after rabbit ear cupping increased by 19.60±2.47 % compared with the image before cupping, indicating an increase in hemoglobin. This signal gradually decreased over time and returned to pre-cupping levels approximately 2 hours later (Fig. 2 A, D). Further calculations revealed that the oxyhemoglobin concentration increased 15 minutes after cupping, with sO_2 increasing by 7.03±1.54 %, following a similar trend as hemoglobin, and returning to pre-cupping levels approximately 2 hours later (Fig. 2B, E). In addition to enhanced PA signals in existing vessels, vessel dilation in the cupping area was observed. By selecting blood vessels of similar thickness in each image, it was found that vessel diameter increased by 56.3±15 % 15 minutes after cupping (Fig. 2A,F). Moreover, the imaging field showed an increase in the number of capillaries. Using binarization methods, VD increased by 66.84±13.7 % 15 minutes after cupping compared to pre-cupping (Fig. 2C,G).

3.2. Cupping therapy with high-pressure (-30 kPa) causes blood vessels rupture and bleeding

When the suction pressure was set to −30 kPa, rabbit ears showed skin ecchymosis after 5 minutes of cupping, similar to what occurs in humans after cupping. Post-cupping imaging revealed significant ecchymosis in the field of view, with no apparent changes within

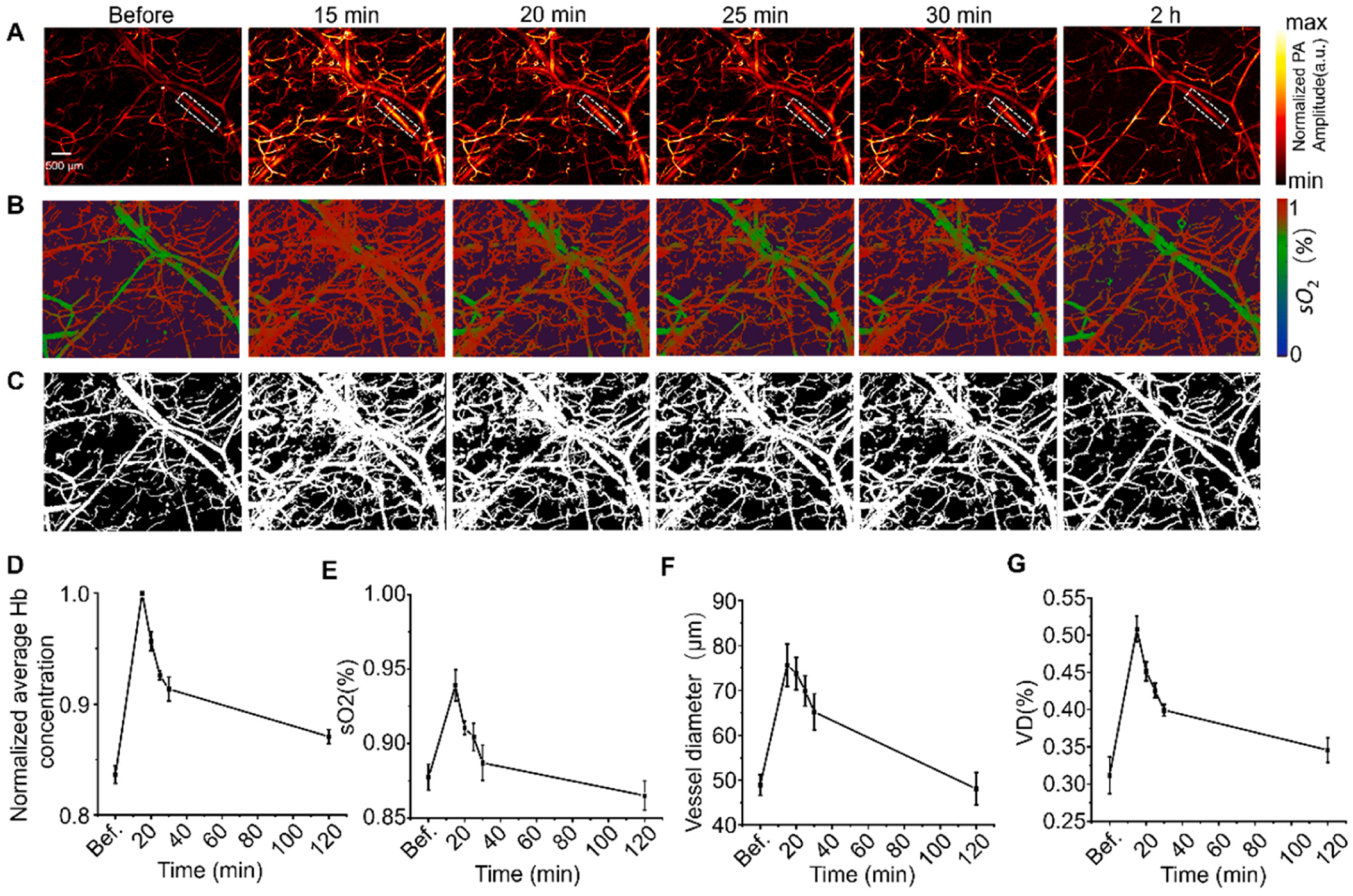

Fig. 2. Cupping therapy with a pressure of −20 kPa promotes blood circulation. (A) Imaging of vascular structure at the cupping site. (B) Imaging of skin oxygenation at the cupping site. (C) Imaging of vascular density at the cupping site. (D) Quantification of average hemoglobin concentration (n=5). (E) Quantification of oxygenation status (n=5). (F) Variation in diameter of the 5 blood vessels within the white dashed line in image A (n=5). (G) Quantification of vascular density (n=5).Data are presented as mean values ± SD.

30 minutes. Subcutaneous tissue edema was observed, causing some tissues and vessels to disappear from view due to being out of focus (Fig. 3A). Over time, the skin edema slowly reduced, tissues gradually returned to their original positions (Fig. 3C). Within 24 hours, edema had largely resolved, revealing more vessels and ecchymosis in the field (Fig. 3A). The area of ecchymosis within the entire imaging field slowly increased as edema resolved, reaching 18.32 % after 24 hours (Fig. 3D). Due to varying degrees of edema post-cupping, we only analyzed images with the highest exposure of bleeding area. The maximum bleeding area observed reached 36.08±15.5 % (n=4). To better delve into the metabolic status of blood oxygen at bleeding sites post-cupping, we delineated a region of interest (ROI) within the bleeding area and calculated the sO_2 of that area. We observed a significant decrease in blood oxygen saturation in the bleeding area post-cupping. The sO_2 decreased from 83.03±1.56 % at half an hour to 64.64±4.11 % after 24 hours (Fig. 3E).

3.3. Cupping therapy with a pressure of −20 kPa facilitates the clearance of ICG through the lymphatic system from a microscopic perspective

We conducted multiple experiments confirming that the maximum absorption peak of ICG is at 780 nm (Fig. 4A). We detected the PA signal amplitude of ICG solutions with different concentrations with PAM at a wavelength of 780 nm (Fig. 4B). The signal amplitude of the ICG solution increased linearly with the concentration of the ICG solution (Fig. 4C), indicating that the average PA signal amplitude generated by ICG is directly proportional to its concentration, that is, the PA signal amplitude reflects the total amount of ICG.

Since the cupping pressure of −30 kPa will cause blood vessels to rupture, resulting in edema at the cupping site, which is obviously not conducive to our observation, we used a cupping pressure of −20 kPa for subsequent lymphatic system observations. Due to the interstitial stress generated by the microneedle injection pressure in the mouse ear, the ICG dye rapidly diffused into the surrounding tissue within 15 minutes after injection. Within 15–30 minutes of subcutaneous injection, ICG was slowly absorbed through the lymphatic system at the injection site.

There was no significant difference in the average PA signal amplitude of ICG in the ears of mice in the control group and mice in the cupping group at 15 and 30 minutes after injection. However, after cupping, the area of ICG in the ear of mice was significantly reduced compared to that of control mice (Fig. 4 E,F), and the average PA signal amplitude in the ICG area was significantly reduced (Fig. 4G). This indicates that the total amount of ICG remaining within the imaging field

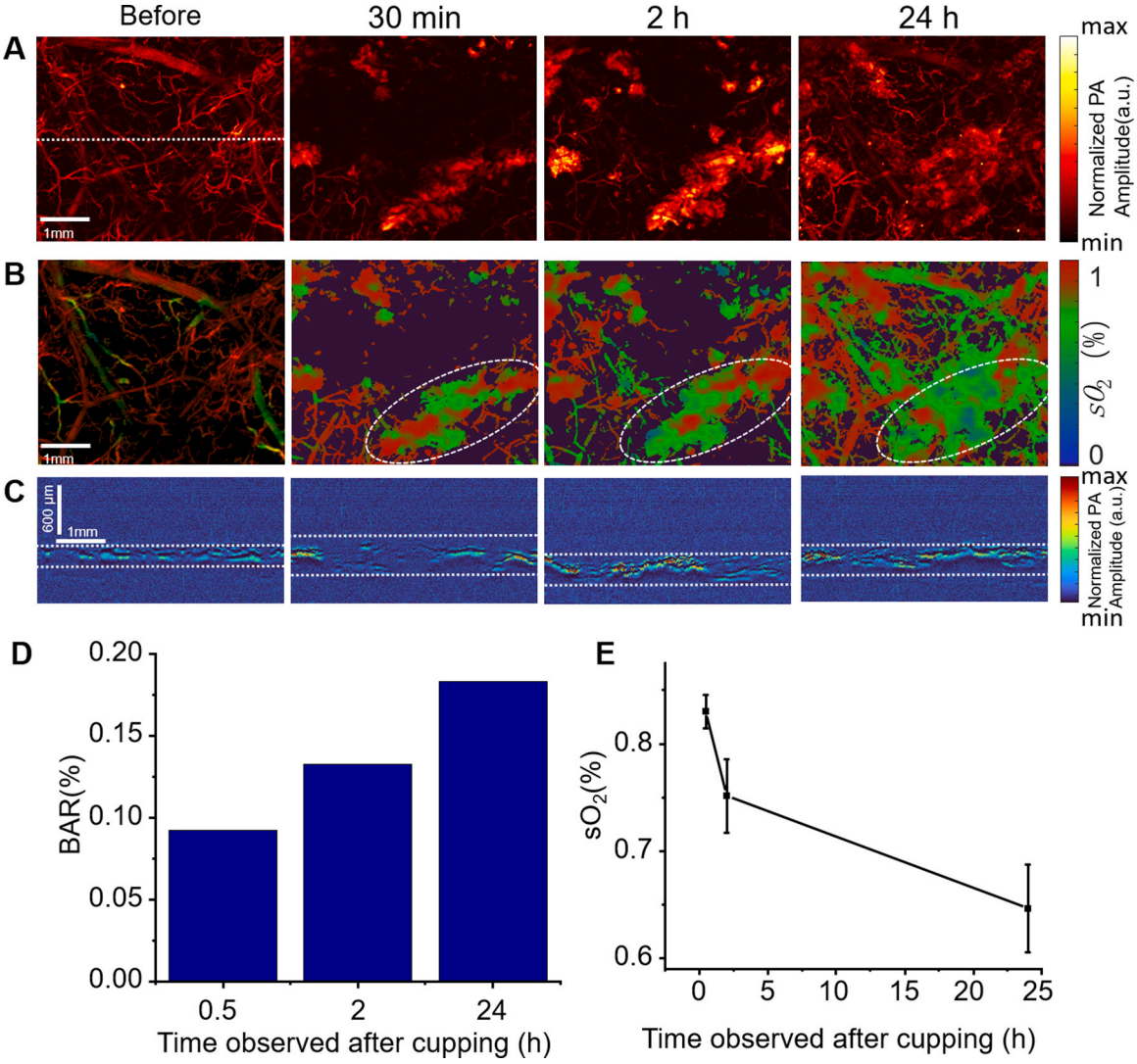

Fig. 3. Cupping therapy with a pressure of −30 kPa can lead to blood vessel rupture, causing hemoglobin to leak into the interstitial space. (A) Imaging of vascular structure at the cupping site. (B) Imaging of skin oxygenation at the cupping site. (C) The B-scan imaging at the white dashed line in image A, the white dotted lines indicate the upper and lower boundaries of the blood vessel signal. (D) Quantification of the bleeding area in image A. (E) Quantification of blood oxygen variations within the white circular region in image B (n=4).Data are presented as mean values ± SD.

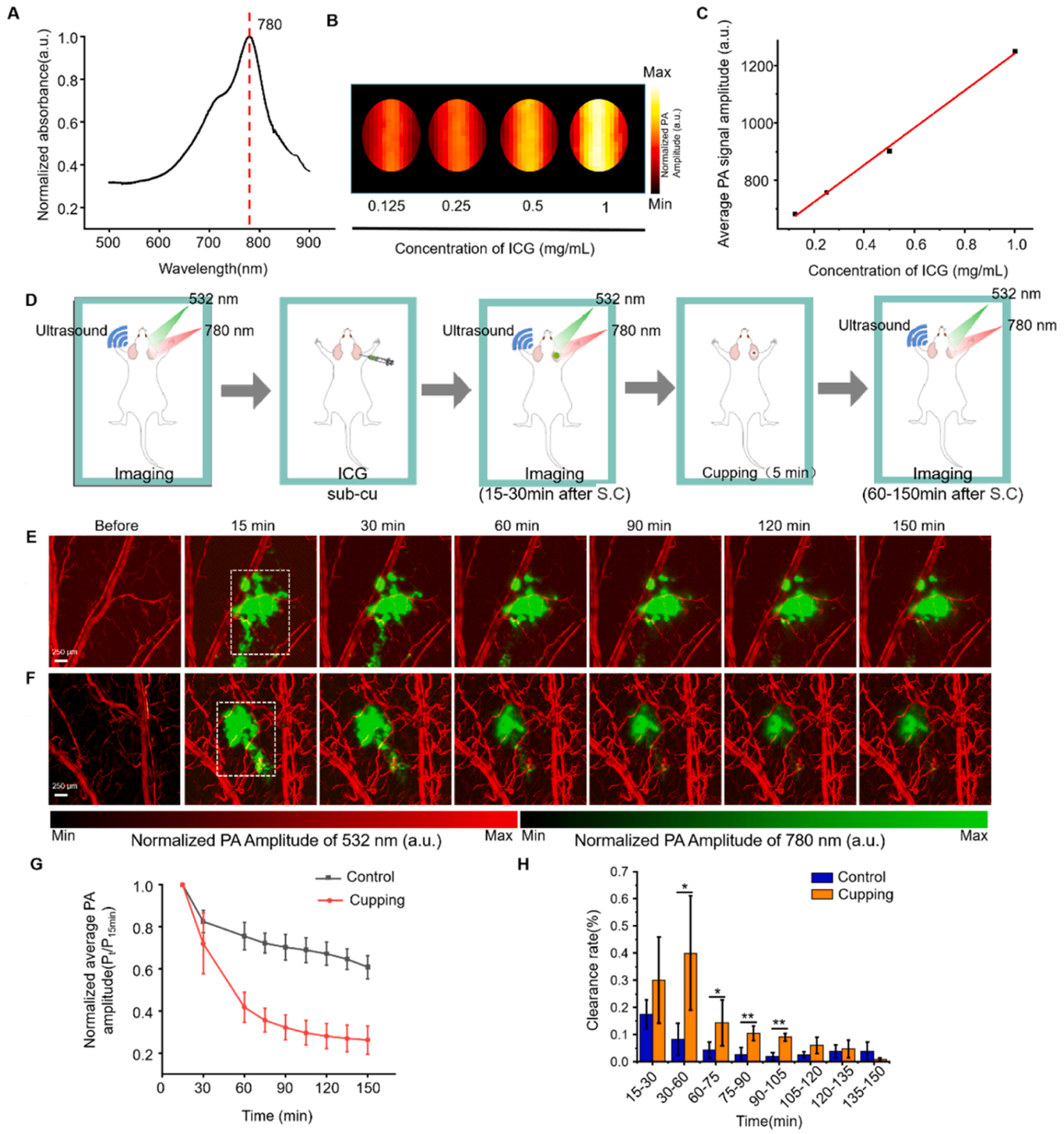

Fig. 4. Cupping with a pressure of −20 kPa promotes ICG clearance through lymphatic channels. (A) The absorption spectrum of ICG. (B) PA Imaging of ICG at different concentrations. (C) Linear dependence of the measured PA signal amplitude on the concentration of ICG. (D) Image workflow diagram. (E,F) Absorption of ICG in ears of mice with cupping therapy and ears of mice without cupping therapy , the red signal represents hemoglobin and the green signal represents ICG solution. (G) Standardization of PA signal amplitude at different time points after ICG injection in the ears of mice with or without cupping therapy, control group: n=6, cupping group: n=5. (H) Clearance rate of ICG at different time points in the ears of mice with or without cupping therapy after ICG injection. Data are presented as mean values ± SD. $^{*}P < 0.05$, $^{**}P < 0.01$.

in the ears of mice in the cupping group was less than that in control mice. We found that the ICG clearance rate in the ears of mice in the cupping group was significantly higher than that of control mice during the periods of 30–60 minutes, 60–75 mins, 75–90 mins, and 90–105 mins (P =0.007 < 0.05,P =0.02 < 0.05, P=0.002 < 0.05, P=0.001 < 0.05) (Fig. 4G), indicating that cupping can promote the clearance of ICG in mouse ears within a short period (within 30–75 minutes after cupping).

3.4. Fluorescence imaging reveals that cupping promotes lymphatic drainage from a macroscopic perspective

We observed the decrease of ICG in the imaging area from the microscopic field of view through PAM. Although subcutaneously injected drugs are often excreted through the lymphatic system, due to the limitations of PAM imaging field of view and resolution, we were unable to track the path of ICG into the lymph nodes. Therefore, we utilized macroscopic fluorescent imaging to observe the impact of cupping therapy on the lymphatic system. In control mice without cupping, ICG entered the ischial lymph nodes 70 minutes after injection into the footpad (Fig. 5 B), whereas in the cupping group, ICG entered the lymph nodes just 10 minutes after injection (Fig. 5 C). The T_{in} time for the cupping group was significantly shorter than that of the control group (P=0.011 < 0.05), indicating that cupping therapy facilitated a faster return of the ICG to the lymph nodes (Fig. 5 F). We detected the brightness of the ischial lymph nodes over 4 hours. The fluorescence intensity of the lymph nodes in the cupping group remained higher than that of the control group after cupping therapy (Fig. 5 D). The SBR of ischial lymph nodes in the cupping group was also significantly higher than that in the control group (Fig. 5E). The T_{max} time of the cupping group was shorter than that of the control (P=0.066>0.05) , suggesting that cupping therapy resulted in more ICG returning to the lymph nodes (Fig. 5 F). From these findings, we conclude that cupping therapy can promote lymphatic drainage.

3.5. Cupping causes loosening of subcutaneous tissue, dilation of blood vessels, and rupture and bleeding

After rabbit ear cupping, the subcutaneous tissue was edematous and showed pathological changes indicative of loose subcutaneous tissue (Fig. 6 A, B). In the cupping group, the subcutaneous tissue became loose, and the distance between hair follicles increased, indicating tissue edema (Fig. 6 C). Pathological tissue showed that after cupping, more red blood cells aggregated in the vascular tissue, and the blood vessels dilated (indicated by the black circles in Fig. 6 B, D), and the blood vessels ruptured and bled. Extravasation of red blood cells into the interstitial space was observed under the skin at both −20 kPa and −30 kPa of cupping (the position indicated by the yellow arrow in Fig. 6 B, D). More red blood cells extravasate into the interstitial space after cupping with a pressure of −30 kPa compared to −20 kPa. This phenomenon was observed both in rabbit ear skin and under mouse skin. In summary, cupping causes blood vessels to dilate and rupture, leading to red blood cells leaking into the interstitial spaces and creating bruises. This is the pathological cause of the cupping marks.

3.6. Cupping therapy improves sepsis outcomes

All mice with sepsis induced by cecal ligation and puncture (CLP) died within 10 hours. Surprisingly, cupping therapy significantly improved the survival rate of septic mice at both −20 kPa and −30 kPa pressures (Fig. 7 A, CLP vs −20 kPa: P=0.0179 < 0.05, CLP vs −30 kPa: P= 0.0064 < 0.01, −20 kPa vs −30 kPa: P= 0.7646 > 0.05). Sepsis

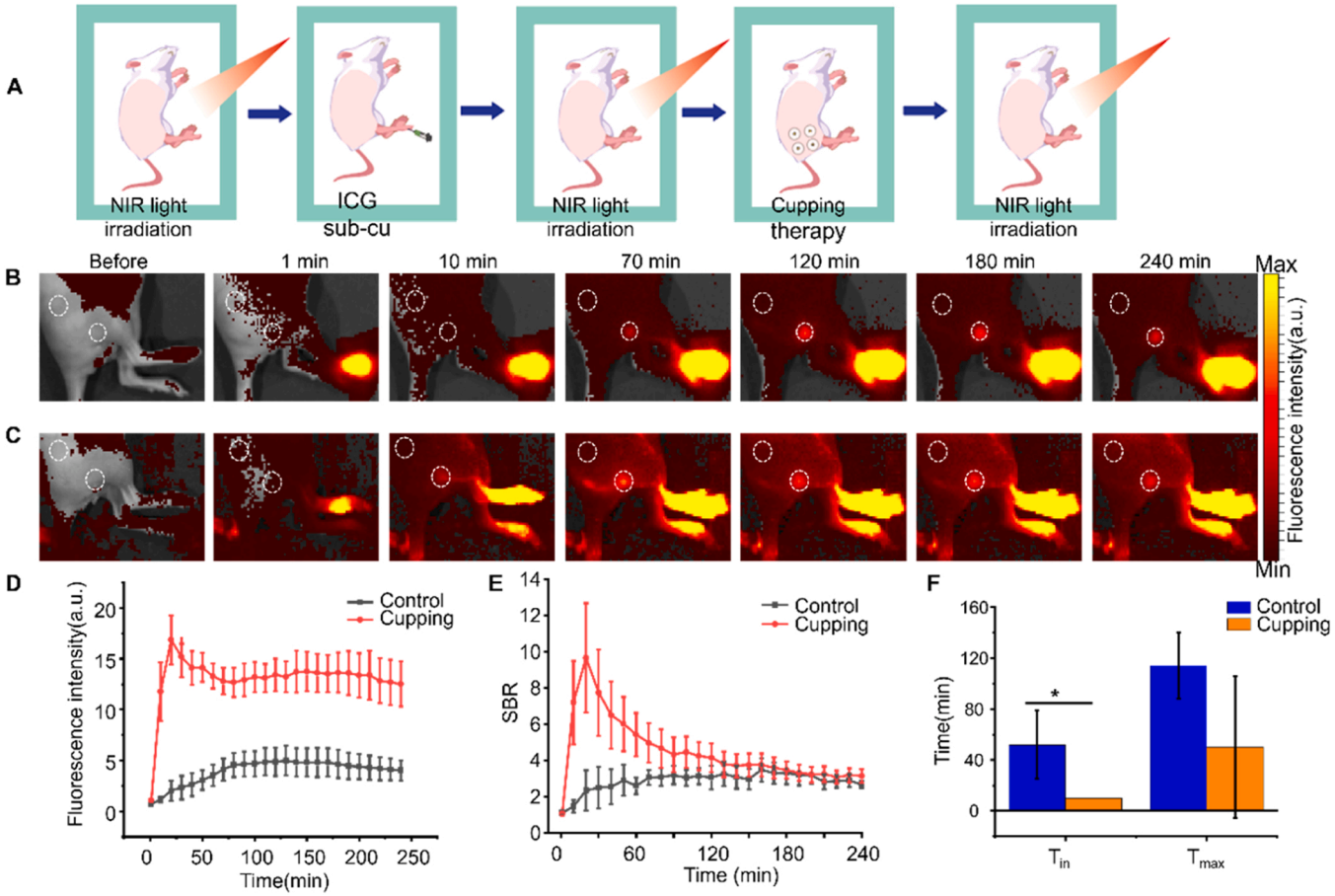

Fig. 5. Cupping therapy with a pressure of −20 kPa promotes lymphatic drainage. (A)Image processing workflow diagram. (B) Fluorescence imaging of the mouse in control group. (C) Fluorescence imaging of the mouse in cupping group. (D) Fluorescence intensity of lymph nodes in the control and cupping groups (Data are presented as mean values ± SEM, control group: n=5, cupping group: n=6). (E) The SBR of the control and cupping groups (Data are presented as mean values ± SEM, control group: n=5, cupping group: n=6). (F) The T_{in} time and T_{max} time of the control and cupping groups. Data are presented as mean values ± SD.

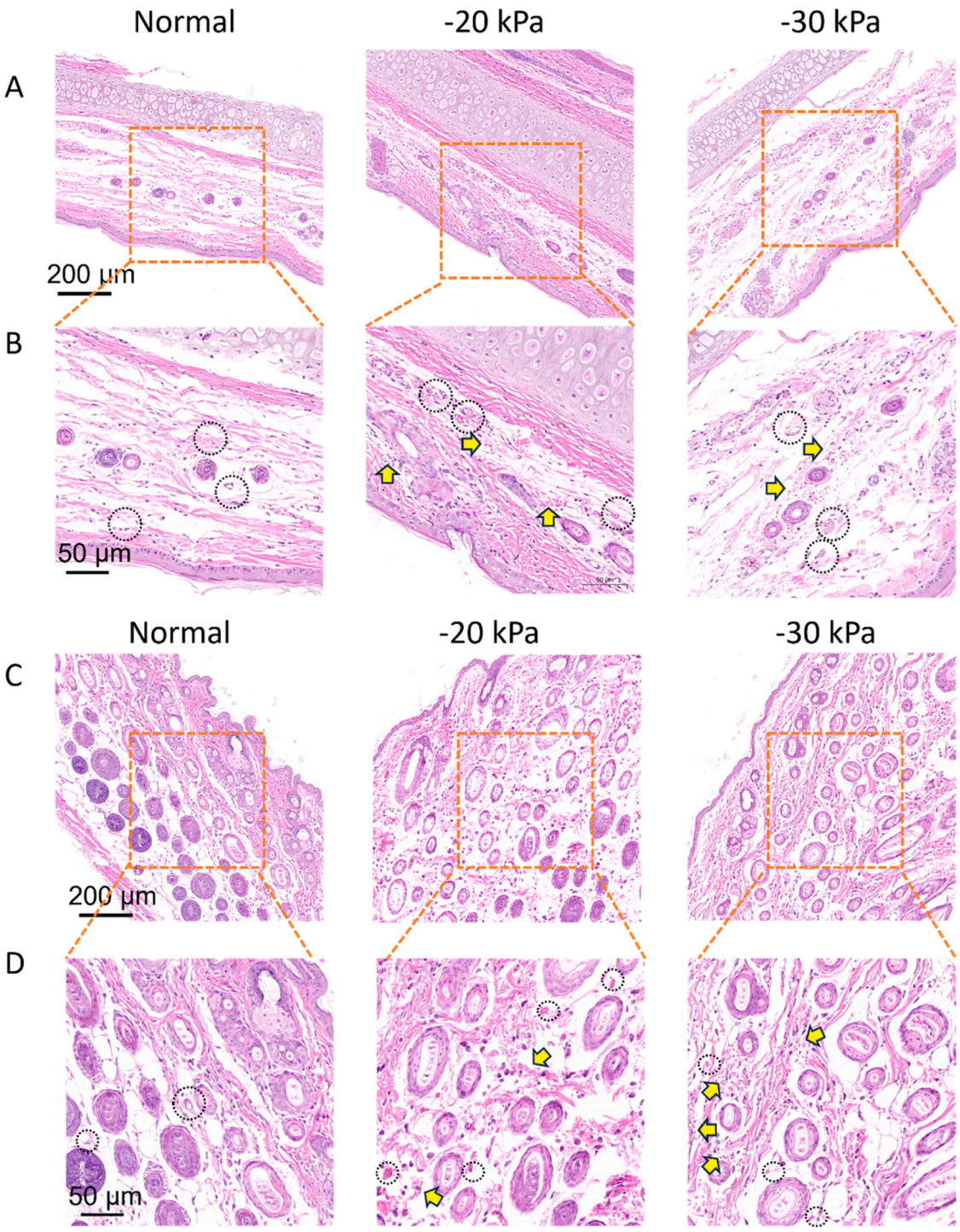

Fig. 6. Pathological examination of normal skin tissue and skin tissue after cupping. (A) H&E staining of rabbits ear skin tissue with or without cupping, bar=200 μm; (B) The enlarged area of the yellow square in figure A, bar=50 μm; (C) H&E staining of dorsal skin tissue of ICR mice with or without cupping, bar=200 μm; (D) The enlarged area of the yellow square in figure C, bar=50 μm. The black circle area indicates blood vessels, and the yellow arrow indicates red blood cells that leak into the tissue space, n=6 in each group.

caused liver function damage, indicated by significant increases in alanine aminotransferase (ALT) and aspartate aminotransferase (AST) levels. Cupping therapy reduced the sepsis-induced elevation of ALT and AST levels, thereby mitigating liver damage (Fig. 7B, C). The effect of sepsis on renal function, as measured by creatinine (Cr) levels, was not significant, and cupping therapy did not produce a noticeable difference (Fig. 7D). Sepsis caused lung tissue damage, such as immune cell infiltration into intercellular spaces, congestion, and increased alveolar wall thickness. Cupping therapy improved sepsis-induced lung damage by reducing inflammatory cell infiltration and alveolar wall thickness (Fig. 7E). Sepsis increased serum inflammatory factors TNF-α, IL-1β, and IL-6 levels. Cupping therapy can reduce serum TNF-α and IL-1β levels, but did not significantly affect IL-6 levels (Fig. 7F, G, H).

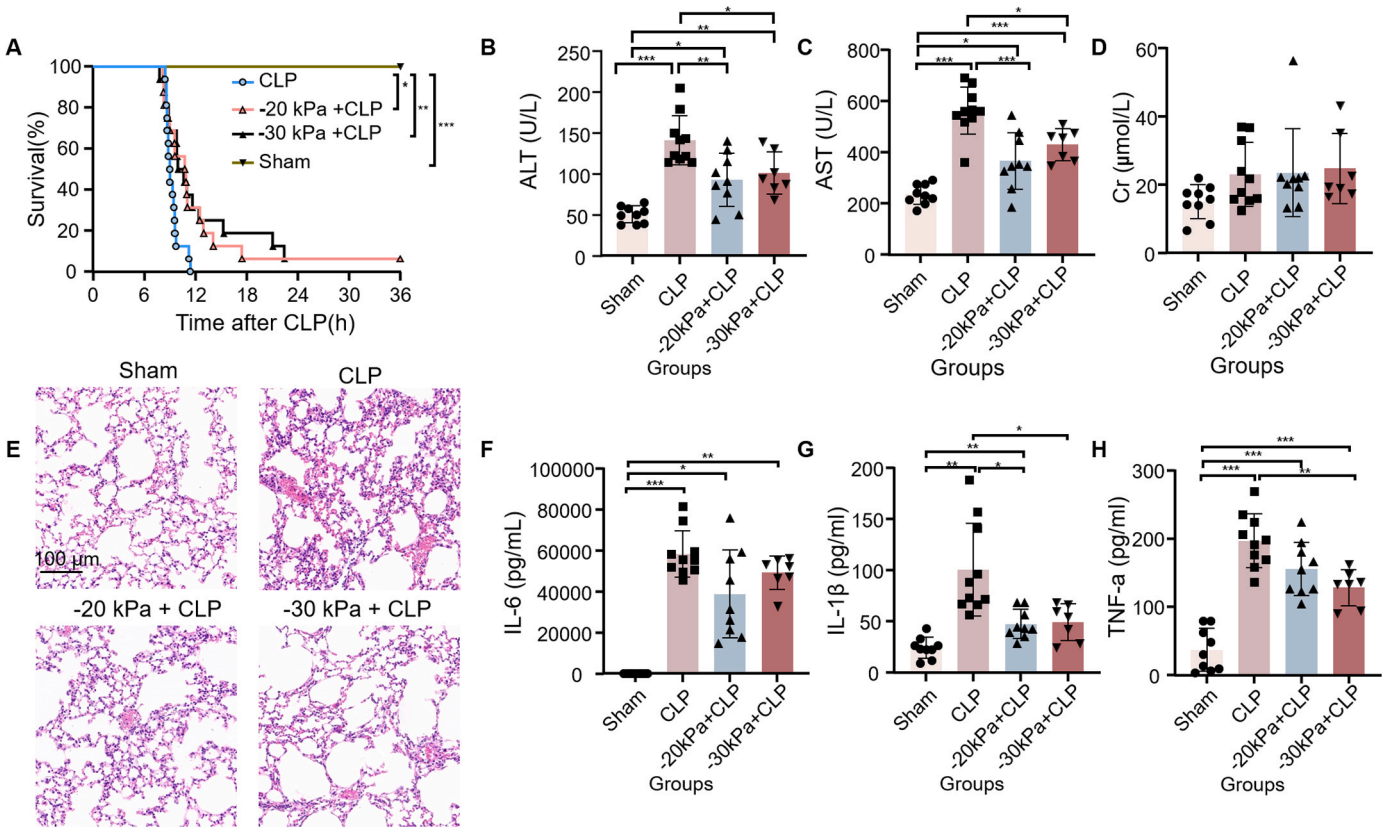

Fig. 7. Cupping therapy improves sepsis outcomes. (A) The survival curve of sham-surgery mice, non-cupping pre-treated group mice and cupping pre-treated mice with −20 kPa or −30 kPa. Sham, n = 6; CLP, n = 16; −20 kPa + CLP, n=16; −30 kPa + CLP, n=16. (B, C, D) Plasma ALT, AST, and Cr levels from sham-surgery mice, non-cupping pre-treated group mice, and cupping pre-treated mice with −20 kPa or −30 kPa pressures. Tissues and blood were harvested when the first mouse became moribund around 7 hours after CLP (n=7–10 in every group). (E) H&E staining of lung tissues from sham-surgery mice, non-cupping pre-treated group mice and cupping pre-treated mice with −20 kPa or −30 kPa. (F, G, H) Quantification of cytokines in the from sham-surgery mice, non-cupping pre-treated group mice and cupping pre-treated mice with −20 kPa or −30 kPa. Data are presented as mean values ± SD, $^{*}P < 0.05$, $^{**}P < 0.01$, $^{***}P < 0.001$.

4. Discussion

In our experiment, we incorporated an external pressure gauge into the electric cupping device to monitor the pressure changes within the cup in real-time. By manual adjustment, we stabilized the internal pressure of the cup at approximately −20 kPa or −30 kPa. The cupping duration was set to 5 minutes based on our experimental findings. A cupping duration of 10 minutes resulted in significant tissue edema, making it impossible to observe the subcutaneous information of the previous imaging depth. Therefore, we decided not to proceed with the 10-minute cupping observation.

Cupping therapy has different effects on the microvasculature under different combinations of cupping therapy pressure and duration. This study employed non-invasive PAM to quantify the microenvironmental changes of cupping therapy at different pressure. We observed that at a cupping pressure of −20 kPa, the average hemoglobin concentration increased, sO_2 levels rose, and blood vessels dilated. Soft tissue within the cup is subjected to tensile stress, while tissue below the cup's edge experiences compressive stress, impeding blood flow within the vasculature. When the cupping pressure was maintained at −20 kPa for 5 minutes, negative pressure application resulted in soft tissue ischemia. Upon cup removal, hemoglobin levels at the cupping site increased rapidly, consistent with previous findings indicating increased local blood flow due to cupping[26]. This blood flow response resembles the reactive hyperemic response to ischemic stress in soft tissue, used clinically to evaluate blood flow function[27]. Larger blood vessels expanded and thickened post-cupping, with microcapillaries becoming visible due to dilation. Vasodilation appears to be the primary mechanism through which cupping enhances blood flow. Increased tissue blood oxygen at the cupping site aligns with Kim et al.'s findings of enhanced tissue oxygenation post-cupping, detected by near-infrared spectroscopy[13]. Unfortunately, we have no way to monitor changes in blood oxygen levels during cupping. Increasing local blood and lymphatic flow through cupping is considered key to relieving myofascial pain[8,28]. Cupping therapy enhances blood flow to the cupped area, delivering more oxygen and nutrients. By improving microcirculation, cupping promotes the repair of capillary endothelial cells, accelerates granulation tissue formation, and stimulates local tissue angiogenesis, which helps relax muscles and restore functional status.

In our experiment, we observed that with a cupping duration of 5 minutes, a pressure of −30 kPa produced markedly different results compared to −20 kPa. Irregular hemoglobin aggregation within the imaging field indicated capillary rupture due to excessive pressure. This excessive pressure caused capillaries to rupture, resulting in hemoglobin leaking into interstitial spaces and forming ecchymoses[29], similar to those observed in humans after cupping. This phenomenon was confirmed in the skin tissues of rabbits and mice. The originally clear blood vessels became obscured due to strong cupping pressure, causing vascular rupture and increased vessel permeability. Consequently, more fluid infiltrated into the interstitial space, leading to interstitial edema. Additionally, the shifting tissue height altered blood vessel positions, rendering them out of focus and undetectable under PAM. Distraction of the skin is believed to increase localized blood flow and enhance tissue healing, reduce perceived pain, and alleviate adhesions within connective tissues[30,31]. As interstitial edema gradually resolved, tissue height normalized, and more blood vessels and bleeding points

reappeared at their pre-edema heights within the imaging field, so bleeding area increased at 24 hours post-cupping compared to half an hour post-cupping. The blood oxygen levels at the bleeding site decreased slowly over time, as erythrocytes in the interstitial space were unable to undergo oxygen exchange, leading to gradual oxygen depletion due to oxygen consumption by tissues.

Currently, it is believed that cupping does not regulate the body's immunity by dilating blood vessels, but that the key to stimulating the body's immune function is the capillary rupture caused by cupping. The widely accepted hypothesis is that cupping causes capillaries at the treatment site to rupture, releasing a large number of signaling molecules and changing the microenvironment[32]. These changes induce immunomodulation by stimulating immune cells to release cytokines and produce neuromodulation by exciting nerve terminals. The interaction between the nervous and immune systems triggers signal amplification, which is transmitted to the central nervous system, activating the neuroendocrine-immune network to achieve overall regulatory functions. In this experiment, we hypothesized that higher cupping pressure would have a better therapeutic effect than lower cupping pressure. To explore the differential effects of varying cupping pressures on the body and quantify their therapeutic impact, we employed a sepsis disease model. Our meticulously designed experiments demonstrated that cupping pretreatment not only enhances the survival rate of septic mice but also protects against sepsis-induced liver and lung damage while reducing serum inflammation levels induced by sepsis[33]. These result underscore the contribution of cupping therapy to understanding the mechanisms and its potential clinical applications in improving outcomes in inflammatory conditions like sepsis. Although liver function and lung tissue pathology results suggest that low-pressure (−20 kPa) cupping may be more efficacious, this advantage is not statistically significant. Consequently, we can only assert that low-pressure (−20 kPa) cupping is sufficient to achieve optimal therapeutic effects.

Prior to these current theories, it was proposed that cupping causes blood vessels to rupture and bleed. Macrophages engulf red blood cells outside the vessels, stimulating the production of heme oxygenase-1 (HO-1). HO-1 catalyzes heme to produce carbon monoxide (CO), biliverdin (BV)/bilirubin (BR), and iron[8]. These products exhibit antioxidant, anti-inflammatory, antiproliferative, and neuromodulatory effects in animal and human systems, and they also stimulate the shift of phagocytes toward an anti-inflammatory M2 phenotype[8,34]. Pathological analysis revealed that cupping pressures of both −20 kPa and −30 kPa caused subcutaneous blood vessels to rupture, resulting in red blood cell extravasation into the tissue space. Regarding efficacy, we found no linear relationship between the size of the ecchymosis or the extent of capillary rupture and the therapeutic effect. Our pressure settings might be inadequate to determine whether low (-20 kPa) or high (-30 kPa) pressure is more beneficial. We can only conclude that the therapeutic effect of cupping at −20 kPa is not less than that of cupping at −30 kPa. Further research is needed to understand the mechanisms by which cupping achieves its therapeutic effects, which is our next challenge.

In this experiment, we demonstrated for the first time that cupping promotes lymphatic reflux, which is measured indirectly due to the lack of specific components in lymph fluid. Studies have shown that particles entering the body through subcutaneous, intramuscular, or intradermal injection primarily enter capillaries when their molecular size is less than 10 nanometers. Larger imaging agents are preferentially cleared through lymphatic capillaries due to interstitial fluid pressure and flow [35]. The flow of exogenous particles from the interstitium to the lymphatic vessels alters the transport mode of imaging agent particles within the lymphatic vessels by changing the interstitial fluid pressure and flow. During subcutaneous injection, fluid is injected into the subcutaneous layer, which increases interstitial pressure, leading to increased lymphatic uptake[36]. ICG is used as a versatile contrast agent for both fluorescence[37] and PA imaging[38]. It is the only near-infrared fluorescent dye approved by the U.S. FDA for clinical applications, known for its safety profile[39,40]. Upon subcutaneous administration, ICG integrates into the lymphatic system, binding with albumin and traversing lymphatic pathways to lymph nodes before reentering the bloodstream. Because the lymphatic system transports slowly, ICG remains in the system for a long time, allowing us to trace draining lymphatic vessels and lymph nodes. Under the PAM field of view, we observed expedited clearance of ICG through the lymphatic system post-cupping. However, despite our efforts, capturing the precise morphology of lymphatic vessels proved difficult, possibly due to solution concentration and the limited sensitivity of the 780 nm probe. To gain further insights into the excretion pathway of ICG, we turned to fluorescence imaging, allowing for a macroscopic perspective of ICG disappearance. After cupping, ICG exhibited accelerated and heightened migration towards ischial lymph nodes. Moreover, a discernible pathway was evident in the cupping group, likely indicative of a lymphatic vessel. Our findings offer compelling evidence of cupping's role in promoting lymphatic drainage.

Our experiment faces certain limitations, primarily due to the imaging depth constraints of our current equipment, which restricts our ability to fully validate the effects of cupping on human skin. Given technical limitations and ethical constraints on human research, animal models were selected as an essential alternative for preliminary investigation. Mice are widely used in traditional Chinese medicine research due to their accessibility and established role in preclinical studies[41,42]. Recognizing the limitations of mouse skin, which is thinner and structurally distinct from human skin, we also used rabbit ears to better simulate cupping's effects on the blood system. Rabbit ears offer a closer approximation to human skin in terms of thickness, although they still cannot fully replicate the complexity of human skin physiology. Therefore, while animal models provide a practical and ethical approach for investigating cupping therapy's effects, we acknowledge that differences in anatomy, physiology, and melanin distribution[43,44] may influence the accuracy of our findings when translating to human clinical contexts. Furthermore, the cupping parameters used in animals (e.g., pressure and duration) require further refinement and validation in human trials, as the dosages applied to animals may not have the same effects in humans. Rigorous ethical and safety evaluations are essential when considering the application of cupping therapy to human subjects. Future clinical studies are necessary to validate these mechanisms and establish the clinical relevance of cupping therapy in humans.

5. Conclusion

In summary, our study has demonstrated that low-pressure cupping (-20 kPa) effectively enhances blood circulation through pressure-induced congestion. Cupping not only boosts tissue blood but also fosters local oxygenation and circulation. Using the exogenous dye ICG, we provided compelling evidence, both microscopically and macroscopically, through PAM and fluorescence imaging, to support cupping's role in promoting lymphatic circulation. This marks the first documented instance of cupping's efficacy in stimulating lymphatic reflux, potentially elucidating its mechanism in alleviating localized pain. Conversely, higher cupping pressure (-30 kPa) may lead to capillary rupture, resulting in blood extravasation into the interstitial space and causing congestion and edema, similar to the bruising observed post-cupping in humans. Our meticulous experimental approach enables the quantification of therapeutic effects under varying cupping pressures. Our findings strongly suggest that the therapeutic efficacy of cupping at −20 kPa is comparable to that achieved with −30 kPa pressure cupping. This study lays the foundation for an objective evaluation of cupping therapy, demonstrating that low-pressure cupping can enhance blood and lymphatic flow while minimizing tissue damage, thus offering a safer treatment method. Future research should further investigate the specific therapeutic effects of different cupping pressures on various diseases and symptoms to optimize clinical applications. Despite the promising results, our study has limitations, as animal

models do not fully replicate human skin. Differences in skin thickness, pigmentation, and anatomy between animals and humans may affect the applicability of these findings. Additionally, the imaging depth of our PAI system limits the full observation of cupping's effects on human skin. Future work will focus on optimizing the PAI system to enhance imaging depth and resolution for clinical applications. Furthermore, the cupping parameters (e.g., pressure and duration) used in this study will require refinement and validation in human trials to ensure safety and efficacy. Ultimately, rigorous clinical studies are needed to confirm these mechanisms and establish the clinical relevance of cupping therapy in human patients, which will be the focus of our next steps.

Funding

This work was supported by grants from National Natural Science Foundation of China (No. 82171931 and 82302253), China Postdoctoral Science Foundation (No. 2023M740773), Guangzhou Municipal Health Commission General Guidance Project (No. 20231A010081).

CRediT authorship contribution statement

Zhu Ai: Writing – review & editing, Resources, Methodology. **Zhehao Wu:** Writing – review & editing, Visualization. **Yang Qiu:** Writing – review & editing, Software, Methodology, Data curation. **Aoji Qin:** Writing – review & editing, Software, Methodology, Data curation. **Liming Nie:** Writing – review & editing, Supervision, Resources, Project administration, Methodology, Formal analysis, Conceptualization. **Zhiming Xiang:** Writing – review & editing, Supervision, Resources, Project administration, Methodology, Funding acquisition, Formal analysis, Conceptualization. **Cuihong Ge:** Writing – review & editing, Writing – original draft, Validation, Methodology, Investigation, Formal analysis, Data curation, Conceptualization. **Bo Yu:** Writing – review & editing, Validation, Methodology, Investigation, Formal analysis. **Ping Zhang:** Writing – review & editing, Writing – original draft, Visualization, Validation, Software, Methodology, Investigation, Formal analysis, Data curation, Conceptualization. **Jing Lv:** Writing – review & editing, Visualization, Validation, Software, Methodology, Investigation, Formal analysis, Data curation, Conceptualization.

Declaration of Competing Interest

The authors declare that they have no known competing financial interests or personal relationships that could have appeared to influence the work reported in this paper.

Acknowledgments

P. Zhang, J. Lv and C. Ge contributed equally to this work. All authors contributed to the study conception and design. All authors read and approved the final manuscript.

Data availability

The data that has been used is confidential.

References

[1] H. Cao, M. Han, X. Li, S. Dong, Y. Shang, Q. Wang, S. Xu, J. Liu, Clinical research evidence of cupping therapy in China: a systematic literature review, J. BMC Complement Alter. Med 10 (2010) 70, https://doi.org/10.1186/1472-6882-10-70.
[2] K. Farhadi, D.C. Schwebel, M. Saeb, M. Choubsaz, R. Mohammadi, A. Ahmadi, The effectiveness of wet-cupping for nonspecific low back pain in Iran: a randomized controlled trial, J. Complement Ther. Med 17 (1) (2009) 9–15, https://doi.org/10.1016/j.ctim.2008.05.003.
[3] L.M. Chi, L.M. Lin, C.L. Chen, S.F. Wang, H.L. Lai, T.C. Peng, The Effectiveness of Cupping Therapy on Relieving Chronic Neck and Shoulder Pain: A Randomized Controlled Trial, J. Evid. Based Complement Altern. Med 2016(1741-427X (Print.)) (2016) 7358918, https://doi.org/10.1155/2016/7358918.
[4] J.I. Kim, M.S. Lee, D.H. Lee, K. Boddy, E. Ernst, Cupping for treating pain: a systematic review, J. Evid. Based Complement Altern. Med 2011 (2011) 467014, https://doi.org/10.1093/ecam/nep035.
[5] H. Cao, C. Zhu, J. Liu, Wet cupping therapy for treatment of herpes zoster: a systematic review of randomized controlled trials, J. Altern. Ther. Health Med. 16 (6) (2010) 48–54.
[6] A.M.N. Al-Bedah, I.S. Elsubai, N.A. Qureshi, T.S. Aboushanab, G.I.M. Ali, A.T. El-Olemy, A.A.H. Khalil, M.K.M. Khalil, M.S. Alqaed, The medical perspective of cupping therapy: Effects and mechanisms of action, J. J. Tradit. Complement. Med. 9 (2) (2019) 90–97, https://doi.org/10.1016/j.jtcme.2018.03.003.
[7] H. Cao, J. Liu, G.T. Lewith, Traditional Chinese Medicine for treatment of fibromyalgia: a systematic review of randomized controlled trials, J. J. Altern. Complement. Med. (N. Y., N. Y.) 16 (4) (2010) 397–409, https://doi.org/10.1089/acm.2009.0599.
[8] D.T. Lowe, Cupping therapy: An analysis of the effects of suction on skin and the possible influence on human health, J. Complement. Ther. Clin. Pract. 29 (2017) 162–168, https://doi.org/10.1016/j.ctcp.2017.09.008.
[9] Y. Tian, S. Wang, G. Wang, S. Jia, X. Song, H. Li, D. Zhang, W. Zhang, [Color spectrum of cupping mark detected by hyperspectral camera:a preliminary observation], J. Zhongguo Zhen Jiu 36 (10) (2016) 1083–1087, https://doi.org/10.13703/j.0255-2930.2016.10.022.
[10] P.-c Xu, S.-l Cui, D.A.C. Wee, S. Xu, L.T. Leang, Preliminary observation on effect of cupping on the skin surface temperature of patients with back pain,J, World J. Acupunct. - Moxibustion 24 (4) (2014) 59–61, http://https://doi.org/10.1016/S1003-5257(15)60030-7.
[11] X. Hou, X. He, X. Zhang, F. Liao, Y.J. Hung, Y.K. Jan, Using laser Doppler flowmetry with wavelet analysis to study skin blood flow regulations after cupping therapy, Ski. Res. Technol. 27 (3) (2021) 393–399, https://doi.org/10.1111/srt.12970.
[12] C. Gao, M. Wang, L. He, Y. He, T. Li, Alternations of hemodynamic parameters during Chinese cupping therapy assessed by an embedded near-infrared spectroscopy monitor, J. Biomed. Opt. Express 10 (1) (2019) 196–203, https://doi.org/10.1364/boe.10.000196.
[13] S. Kim, E. Kim, G. Jung, S. Lee, J.G. Kim, The hemodynamic changes during cupping therapy monitored by using an optical sensor embedded cup,J, J. biophotonics 12 (5) (2019) e201800286, https://doi.org/10.1002/jbio.201800286.
[14] Y. Zhou, F. Cao, H. Li, X. Huang, D. Wei, L. Wang, P. Lai, Photoacoustic imaging of microenvironmental changes in facial cupping therapy,J, Biomed. Opt. Express 11 (5) (2020) 2394–2401, https://doi.org/10.1364/boe.387985.
[15] Y. Liu, L. Nie, X. Chen, Photoacoustic Molecular Imaging: From Multiscale Biomedical Applications Towards Early-Stage Theranostics, J. Trends Biotechnol. 34 (5) (2016) 420–433, https://doi.org/10.1016/j.tibtech.2016.02.001.
[16] W. Pang, B. Zhu, H. Li, Y. Zhou, C.M. Woo, X. Huang, T. Zhong, H. Lo, L. Wang, P. Lai, Direct Monitoring of Whole-Brain Electrodynamics via High-Spatiotemporal-Resolution Photoacoustics with Voltage-Sensitive Dye,J, Laser Photonics Rev. (2024) 2400165.
[17] H.F. Zhang, K. Maslov, G. Stoica, L.V. Wang, Functional photoacoustic microscopy for high-resolution and noninvasive in vivo imaging, J. Nat. Biotechnol. 24 (7) (2006) 848–851, https://doi.org/10.1038/nbt1220.
[18] X. Wang, Y. Pang, G. Ku, X. Xie, G. Stoica, L.V. Wang, Noninvasive laser-induced photoacoustic tomography for structural and functional in vivo imaging of the brain, J. Nat. Biotechnol. 21 (7) (2003) 803–806, https://doi.org/10.1038/nbt839.
[19] S. Gong, Z. Yan, Z. Liu, M. Niu, H. Fang, N. Li, C. Huang, L. Li, G. Chen, H. Luo, X. Chen, H. Zhou, J. Hu, W. Yang, Q. Huang, B. Schnabl, P. Chang, T.R. Billiar, Y. Jiang, P. Chen, Intestinal Microbiota Mediates the Susceptibility to Polymicrobial Sepsis-Induced Liver Injury by Granisetron Generation in Mice, J. Hepatol. (Baltim., Md.) 69 (4) (2019) 1751–1767, https://doi.org/10.1002/hep.30361.
[20] X. Chen, R. Wu, L. Li, Y. Zeng, J. Chen, M. Wei, Y. Feng, G. Chen, Y. Wang, L. Lin, H. Luo, A. Chen, Z. Zeng, F. He, Y. Bai, S. Zhang, Y. Han, Z. Wang, X. Zhao, W. Xiao, Y. Jiang, S. Gong, Pregnancy-induced changes to the gut microbiota drive macrophage pyroptosis and exacerbate septic inflammation, e9, J. Immun. 56 (2) (2023) 336–352, https://doi.org/10.1016/j.immuni.2023.01.015.
[21] J. Yao, L.V. Wang, Sensitivity of photoacoustic microscopy, J. Photoacoust. 2 (2) (2014) 87–101, https://doi.org/10.1016/j.pacs.2014.04.002.
[22] T. Wang, N. Sun, R. Cao, B. Ning, R. Chen, Q. Zhou, S. Hu, Multiparametric photoacoustic microscopy of the mouse brain with 300-kHz A-line rate, J. Neurophotonics 3 (4) (2016) 045006, https://doi.org/10.1117/1.NPh.3.4.045006.
[23] G. Huang, J. Lv, Y. He, J. Yang, L. Zeng, L. Nie, In vivo quantitative photoacoustic evaluation of the liver and kidney pathology in tyrosinemia, J. Photoacoust. 28 (2022) 100410, https://doi.org/10.1016/j.pacs.2022.100410.
[24] J. Zhang, X. Sun, H. Li, H. Ma, F. Duan, Z. Wu, B. Zhu, R. Chen, L. Nie, In vivo characterization and analysis of glioblastoma at different stages using multiscale photoacoustic molecular imaging, J. Photoacoust. 30 (2023) 100462, https://doi.org/10.1016/j.pacs.2023.100462.
[25] A. Khadria, C.D. Paavola, K. Maslov, F.A. Valenzuela, A.E. Sperry, A.L. Cox, R. Cao, J. Shi, P.L. Brown-Augsburger, E. Lozano, R.L. Blankenship, R. Majumdar, S. A. Bradley, J.M. Beals, S.S. Oladipupo, L.V. Wang, Photoacoustic imaging reveals mechanisms of rapid-acting insulin formulations dynamics at the injection site, J. Mol. Metab. 62 (2022) 101522, https://doi.org/10.1016/j.molmet.2022.101522.
[26] X. He, X. Zhang, F. Liao, L. He, X. Xu, Y.K. Jan, Using reactive hyperemia to investigate the effect of cupping sizes of cupping therapy on skin blood flow

responses, J. J. back Musculoskelet. Rehabil. 34 (2) (2021) 327–333, https://doi.org/10.3233/bmr-200120.
[27] R.J. Wang, C. Xu, H.F. Tang, Reactive hyperemia index as an integrated marker in prediction of bleeding and cardiovascular death in ACS, J. Int. J. Cardiol. 382 (2023) 85–86, https://doi.org/10.1016/j.ijcard.2023.03.045.
[28] D.C. Sloas, S.A. Stewart, R.S. Sweat, T.M. Doggett, N.G. Alves, J.W. Breslin, D. P. Gaver, W.L. Murfee, Estimation of the Pressure Drop Required for Lymph Flow through Initial Lymphatic Networks, J. Lymphat. Res. Biol. 14 (2) (2016) 62–69, https://doi.org/10.1089/lrb.2015.0039.
[29] L.M. Tham, H.P. Lee, C. Lu, Cupping: from a biomechanical perspective, J. J. Biomech. 39 (12) (2006) 2183–2193, https://doi.org/10.1016/j.jbiomech.2005.06.027.
[30] L.M. Chi, L.M. Lin, C.L. Chen, S.F. Wang, H.L. Lai, T.C. Peng, The Effectiveness of Cupping Therapy on Relieving Chronic Neck and Shoulder Pain: A Randomized Controlled Trial, J. Evid. Based Complement Altern. Med 2016 (2016) 7358918, https://doi.org/10.1155/2016/7358918.
[31] M.S. Lee, T.Y. Choi, B.C. Shin, J.I. Kim, S.S. Nam, Cupping for hypertension: a systematic review, J. Clin. Exp. Hypertens. (N. Y., N. Y.: 1993) 32 (7) (2010) 423–425, https://doi.org/10.3109/10641961003667955.
[32] Y. Guo, B. Chen, D.Q. Wang, M.Y. Li, C.H. Lim, Y. Guo, Z. Chen, Cupping regulates local immunomodulation to activate neural-endocrine-immune worknet, J. Complement. Ther. Clin. Pract. 28 (2017) 1–3, https://doi.org/10.1016/j.ctcp.2017.04.005.
[33] Q. Zhang, X. Wang, G. Yan, J. Lei, Y. Zhou, L. Wu, T. Wang, X. Zhang, D. Ye, Y. Li, Anti- Versus Pro-Inflammatory Metabololipidome Upon Cupping Treatment, J. Cell. Physiol. Biochem.: Int. J. Exp. Cell. Physiol., Biochem., Pharmacol. 45 (4) (2018) 1377–1389, https://doi.org/10.1159/000487563.
[34] I. Nakamichi, A. Habtezion, B. Zhong, C.H. Contag, E.C. Butcher, M.B. Omary, Hemin-activated macrophages home to the pancreas and protect from acute pancreatitis via heme oxygenase-1 induction, J. J. Clin. Investig. 115 (11) (2005) 3007–3014, https://doi.org/10.1172/jci24912.
[35] P. Zbyszynski, I. Toraason, L. Repp, G.S. Kwon, Probing the subcutaneous absorption of a PEGylated FUD peptide nanomedicine via in vivo fluorescence imaging, J. Nano Converg. 6 (1) (2019) 22, https://doi.org/10.1186/s40580-019-0192-3.
[36] N.L. Trevaskis, L.M. Kaminskas, C.J. Porter, From sewer to saviour - targeting the lymphatic system to promote drug exposure and activity, J. Nat. Rev. Drug Discov. 14 (11) (2015) 781–803, https://doi.org/10.1038/nrd4608.
[37] M.-L. Li, J.-T. Oh, X. Xie, G. Ku, W. Wang, C. Li, G. Lungu, G. Stoica, L.V. Wang, Simultaneous molecular and hypoxia imaging of brain tumors in vivo using spectroscopic photoacoustic tomography, J. Proc. IEEE 96 (3) (2008) 481–489.
[38] C. Kim, K.H. Song, F. Gao, L.V. Wang, Sentinel lymph nodes and lymphatic vessels: noninvasive dual-modality in vivo mapping by using indocyanine green in rats–volumetric spectroscopic photoacoustic imaging and planar fluorescence imaging, J. Radiol. 255 (2) (2010) 442–450, https://doi.org/10.1148/radiol.10090281.
[39] W. Feindel, Y. Yamamoto, P. Hodge, The human cerebral microcirculation studied by intra-arterial radio-active tracers, Coomassie Blue and fluorescein dyes, J. Bibl. Anat. 9 (1967) 220–224.
[40] M.B. Reinhart, C.R. Huntington, L.J. Blair, B.T. Heniford, V.A. Augenstein, Indocyanine Green: Historical Context, Current Applications, and Future Considerations, J. Surg. Innov. 23 (2) (2016) 166–175, https://doi.org/10.1177/1553350615604053.
[41] S. Liu, Z. Wang, Y. Su, L. Qi, W. Yang, M. Fu, X. Jing, Y. Wang, Q. Ma, A neuroanatomical basis for electroacupuncture to drive the vagal-adrenal axis,J, Nature 598 (7882) (2021) 641–645, https://doi.org/10.1038/s41586-021-04001-4.
[42] L. Yao, Q. Ye, Y. Liu, S. Yao, S. Yuan, Q. Xu, B. Deng, X. Tang, J. Shi, J. Luo, J. Wu, Z. Wu, J. Liu, C. Tang, L. Wang, N. Xu, Electroacupuncture improves swallowing function in a post-stroke dysphagia mouse model by activating the motor cortex inputs to the nucleus tractus solitarii through the parabrachial nuclei, J. Nat. Commun. 14 (1) (2023) 810, https://doi.org/10.1038/s41467-023-36448-6.
[43] T.R. Else, L. Hacker, J. Gröhl, E.V. Bunce, R. Tao, S.E. Bohndiek, Effects of skin tone on photoacoustic imaging and oximetry,J, J. Biomed. Opt. 29 (1) (2024) S11506, https://doi.org/10.1117/1.Jbo.29.S1.S11506.
[44] Y. Mantri, J.V. Jokerst, Impact of skin tone on photoacoustic oximetry and tools to minimize bias,J, Biomed. Opt. Express 13 (2) (2022) 875–887, https://doi.org/10.1364/boe.450224.

Ping Zhang is a doctoral student at Guangzhou University of Chinese Medicine. Her research interests are the applications of photoacoustic imaging in quantitative evaluation and mechanism exploration in traditional Chinese medicine treatment.

Jing Lv is a postdoctoral fellow of Research Center of Medical Sciences of Guangdong Provincial People's Hospital, Guangdong Academy of Medical Sciences. She got his Ph.D. degree from Xiamen University, China in 2022. Her main research interests are the structural and functional photoacoustic imaging application of metabolic related disease models as well as contrast-enhanced quantitative, dynamic, metabolic imaging of livers and kidneys.

Cuihong Ge is a doctoral student at Guangzhou University of Chinese Medicine. She specializes in the mechanism of traditional Chinese medicine in the treatment of respiratory diseases.

Bo Yu is a doctoral candidate at the Second Affiliated Hospital of Harbin Medical University. Her research focuses on the development of nanomaterial imaging.

Yang Qiu is a master's student at Southern Medical University. His research interests primarily focus on developing photoacoustic microscopy systems capable of imaging at greater depths.

Aoji Qin is a master's student at Southern Medical University. His research interest lies in digital image processing and program design.

Zhu Ai is an attending physician at the Department of Radiology, Panyu Central Hospital affliated to Guangzhou Medical University. Her research interest is centered on leveraging artificial intelligence for advancements in tumor diagnosis.

Zhehao Wu is a master's student at Guangzhou University of Chinese Medicine. His research focuses on the application of algorithms related to coronary CT angiography.

Liming Nie is a professor and Ph.D. supervisor at Research Center of Medical Sciences of Guangdong Provincial People's Hospital, Guangdong Academy of Medical Sciences. His laboratory focuses on optical imaging technology, mainly on photoacoustic microscopy, photoacoustic computed tomography, and other related imaging modalities. One of his aims is to provide effective and low-cost imaging instruments for disease diagnosis and treatment monitoring.

Zhiming Xiang is a professor and Ph.D. supervisor in Postgraduate cultivation base of Guangzhou University of Chinese Medicine, Panyu Central Hospital. His laboratory focuses on using artificial intelligence to enhance traditional medical imaging technologies, such as CT and MRI, for diagnostic purposes. He places a particular emphasis on early tumor diagnosis, especially in the study of liver and lung cancers.